Journal of Composite Materials

http://jcm.sagepub.com

Analysis of Mode I and Mode II Tests for Composites with Translaminar Reinforcements

Leishan Chen, Peter G. Ifju and Bhavani V. Sankar

Journal of Composite Materials 2005; 39; 1311
DOI: 10.1177/0021998305050425

The online version of this article can be found at:
http://jcm.sagepub.com/cgi/content/abstract/39/15/1311

Published by:
SAGE
http://www.sagepublications.com

On behalf of:
American Society for Composites

Analysis of Mode I and Mode II Tests for Composites with Translaminar Reinforcements

LEISHAN CHEN, PETER G. IFJU AND BHAVANI V. SANKAR*
Department of Mechanical and Aerospace Engineering
University of Florida
PO Box 116250, Gainesville
FL 32611-6250, USA

(Received November 24, 2003)
(Accepted October 13, 2004)

ABSTRACT: This paper presents finite element models to determine the Mode I and Mode II fracture toughness of stitched composites in conjunction with experiments. Two new test methods to measure the Mode I and Mode II fracture toughness of stitched composites are developed. From the experimental load–deflection diagram, the effective fracture toughness can be determined by the area method. However, in order to comprehensively understand the effect of stitches, two parameters, $G_{c\text{-}par}$ (parent material's fracture toughness) and $G_{c\text{-}eff}$ (effective fracture toughness) are needed to represent the fracture behavior of stitched composites. $G_{c\text{-}par}$ is the intrinsic property of the parent material and is independent of stitch behavior. $G_{c\text{-}eff}$ is the effective critical strain energy release rate that includes the effects of stitching. The purpose of performing the finite element analysis is to identify the correct physical models that represent the stitch interactions with the parent laminate and stitch failure mechanisms. $G_{c\text{-}par}$ and $G_{c\text{-}eff}$ can be obtained through different paths of the J-integral in the FE models. The models help in understanding the effects of stitch stiffness and spacing on the fracture toughness without the need for fabricating and testing stitched composite specimens.

KEY WORDS: finite element model, fracture toughness, J-integral, laminated composites, mode I fracture, mode II fracture, stitching, translaminar reinforcements.

INTRODUCTION TO MODE I TESTING

GRAPHITE/EPOXY LAMINATED COMPOSITES have very high strength-to-weight and stiffness-to-weight ratios. They have tremendous advantages over the conventional materials in many applications, such as aerospace and automotive structures, in which the aforementioned properties are critical. Also, fiber-reinforced composite materials can easily

*Author to whom correspondence should be addressed. E-mail: sankar@ufl.edu

0021-9983/05/15 1311–23 $10.00/0 DOI: 10.1177/0021998305050425

be tailored to obtain desired properties in different directions and can be optimized to meet specific performance requirements. However, these materials suffer a big deficiency – lack of through-the-thickness reinforcement. Fracture toughness of these materials is so low that as crack is initiated between the layers, the delamination can propagate easily. Through-the-thickness stitching is considered one of the ways to reinforce the laminated composites and prevent crack propagation.

Mignery et al. [1] investigated the use of stitching with Kevlar® yarns to suppress delamination in graphite/epoxy laminates. Results showed that stitches effectively arrested delamination. Dexter and Funk [2] characterized the impact resistance and interlaminar fracture toughness of quasi-isotropic graphite-epoxy laminates made of unidirectional Thornel 300-6K fibers/Hercules 3501-6 resin and stitched with polyester and Kevlar yarns. They experimented with stitch parameters and found a significant drop in damage areas of stitched laminates compared to unstitched laminates for the same impact energy. The Mode I fracture toughness, characterized by the critical strain energy release rate, G_{Ic}, was found to be about 30 times higher for the stitched laminates. Ogo [3] investigated the effect of through-the-thickness stitching of plain woven graphite/epoxy laminates with Kevlar yarn. The study showed a manifold increase in G_{Ic} values at the expense of a slight drop in the in-plane properties. Pelstring and Madan [4] developed semiempirical formulae relating damage tolerance of composite laminates to stitch parameters. Mode I critical strain energy release rate was found to be 15 times greater than in unstitched laminates. Critical strain energy release rates decreased exponentially with increased stitch spacing. Dransfield et al. [5] investigated the effect of through-the-thickness stitching of plain woven graphite/epoxy laminates with Kevlar® yarns. Their study showed a manifold increase in G_{Ic} values at the expense of a slight drop in the in-plane properties. Sharma and Sankar [6] conducted a study on the effects of stitching on interlaminar fracture toughness of uniweave textile composites. They used the double cantilever beam setup to test low density stitched specimens and the University of Florida Compression-After-Impact (UF-CAI) test fixture to investigate effects of stitching on sublaminate buckling behavior. Their study showed that stitching had a profound effect on Mode I fracture toughness and CAI strength. They also found that stitching does not increase the impact load at which delamination begins to propagate, but greatly reduces the extent of delamination growth at the end of the impact event. Jain et al. [7–9] used the double cantilever beam (DCB) test for stitched composites and found that the cantilever arms failed in bending before crack propagation. They used aluminum bars to bond the surfaces of the specimen to reinforce the specimen to prevent the specimen arms from failing during the DCB tests. A comparison of the specimens with tabs and without tabs showed that tabs altered the failure mechanism of the stitched thread, and that the improvement in Mode I delamination toughness was underestimated. The fracture toughness of stitched composites had 10-fold improvement. Sankar and Dharmapuri [10] presented an analytical model to simulate stitched laminates and also found that Mode I fracture toughness increases dramatically due to stitching. However, as the stitch density increases or the strength of a stitch increases, the standard DCB setup cannot be used because the specimen fails prior to crack propagation. Failure occurred as a result of compressive instability derived from the high bending moment required for crack propagation. This resulted in the failure of one of the arms of the DCB specimen.

After carefully studying the failure mechanism of the stitched specimens, Chen et al. [11–13] proposed a conceptual solution for Mode I testing of heavily stitched specimens. A new fixture was developed as illustrated in Figure 1. The transverse component of the

force acts to open the crack while the axial component acts to suppress the compressive instability by applying a tensile force. The fixture was designed such that the initial angles of the arms can be adjusted for a given stitched specimen. The loading condition of a specimen is shown in Figure 2. One end of the specimen is clamped and all the forces from the loading fixture can be moved to the cross sections A and A′. The load is monitored by a load cell and the displacement is obtained from the crosshead. Figure 3 shows the load

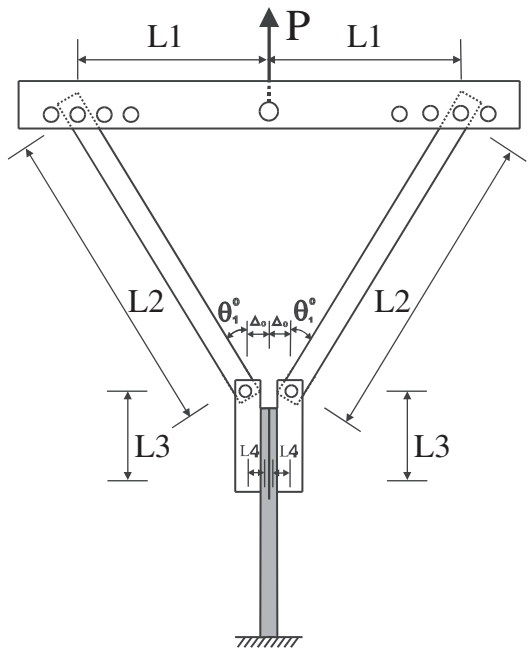

Figure 1. *The new Mode I delamination test setup for stitched laminates.*

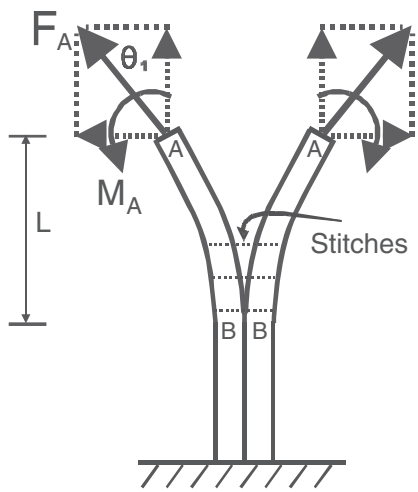

Figure 2. *Loads acting on the specimen in Mode I test.*

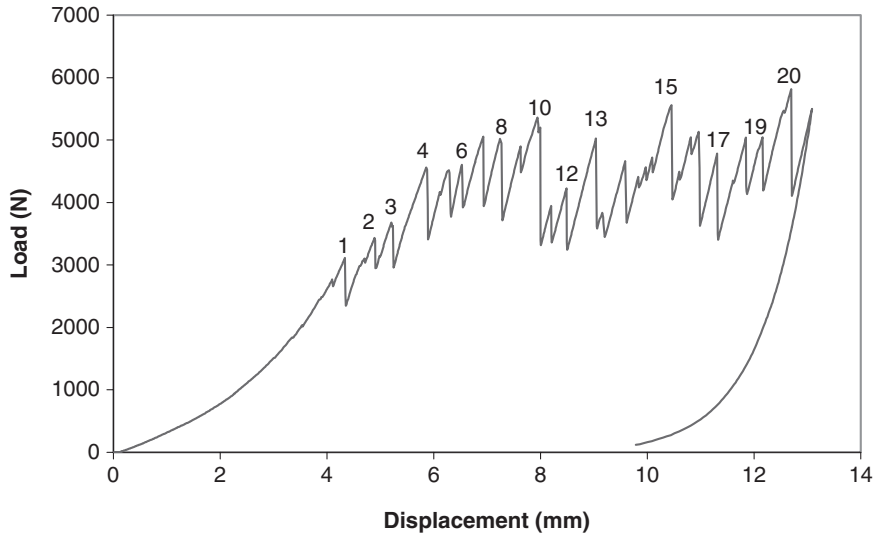

Figure 3. *Load vs displacement diagram of a stitched specimen tested using the fixture shown in Figure 1. Each peak load corresponds to a row of broken stitches.*

versus displacement diagram of this setup. The fixture unzips the stitches one by one and crack propagation is found to be stable.

INTRODUCTION TO MODE II TESTING

A study by Sharma and Sankar [6] showed that Mode II fracture toughness of stitched specimens increases with the delamination area bridged by stitches. They showed that in Mode II loading, stitches do not break as widely expected, but deform the surrounding matrix. This deformation absorbs energy from the system and increases the Mode II fracture toughness. Mode I and Mode II fracture studies by Sharma and Sankar [6] were concerned only with uniweaves, wherein stitch rows ran parallel to the fiber direction. Their study indicated that the interactions among stitches, fibers, and the matrix phase of the parent laminate were quite complicated. Jain and Mai [14] used two specimen geometries: end-notch flexure (ENF) and an end-notch cantilever geometry to analyze the effect of stitching on Mode II delamination toughness. They found that the effect of stitching on both specimen geometries was the same. Massabo and Cox [15] used the crack bridging concept to study the effect of stitching in Mode II delamination. Jain et al. [16] investigated the Mode II delamination toughness by using an end-notched flexure specimen and found that the application of the load to the unstitched specimens caused the initial delamination to grow in an unstable manner. However, the delamination growth was stable in stitched laminates. The improvement due to stitching was in the range of 100–200% with respect to unstitched specimens. It was also observed that increasing stitch thread diameter or stitch density generally led to larger improvement in Mode II toughness. Sharma and Sankar [6] used three approaches (area method, equivalent area method, and classical beam theory) to calculate G_{IIc}.

They determined the location of the crack tip using an optical microscope as well as ultrasonic C-scan. Results showed that an increase in apparent G_{IIc} of stitched composites was 5–15 times depending on the extent of crack propagation. The stitches did not break during these tests. Clara and Barry [17] investigated the accuracy of the four-point bending end-notched flexure (4ENF) test for determining Mode II delamination toughness. Results showed that the 4ENF test yields toughness values similar to that obtained by ENF testing. The ENF tests performed by many researchers [18–22] showed that stitching indeed increases the delamination toughness of composites. However, because of the limitations of the ENF setup, a fully developed bridging zone is never achieved. Thus, the instantaneous strain energy release rate changes as the crack propagates. Chen et al. [23] used a new setup (cantilever beam setup) to obtain much longer crack lengths. They incorporated high sensitivity Moiré interferometry [24] to determine the location of the crack tip and the relative displacement of the two crack surfaces.

The cantilever beam setup is shown in Figure 4. The length of a specimen for this setup was 178 mm long and 25.4 mm wide. A grating, required for Moiré interferometry, was replicated on the edge of the specimen. The high sensitivity Moiré interferometry setup was used to accurately locate the crack tip and the displacement field after crack propagation. Using this setup, one can obtain more than 50 mm of the crack extension, which is equivalent to 16 rows of stitches in a high-density specimen (6.2 stitches/cm^2) or eight rows of stitches in a low stitch density specimen (3.1 stitches/cm^2). A typical load versus displacement diagram of the cantilever ENF test is shown in Figure 5. One can see that the slope of the load–displacement curve is almost constant before the load reaches the critical value of ≈178 N. However, as the load increases, the slope gradually decreases as the rigidity of the beam decreases due to crack propagation.

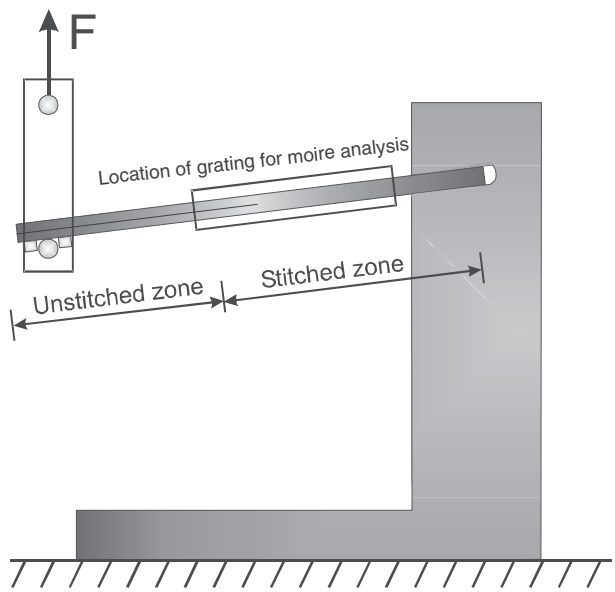

Figure 4. *Schematic of the cantilever beam setup for Mode II test.*

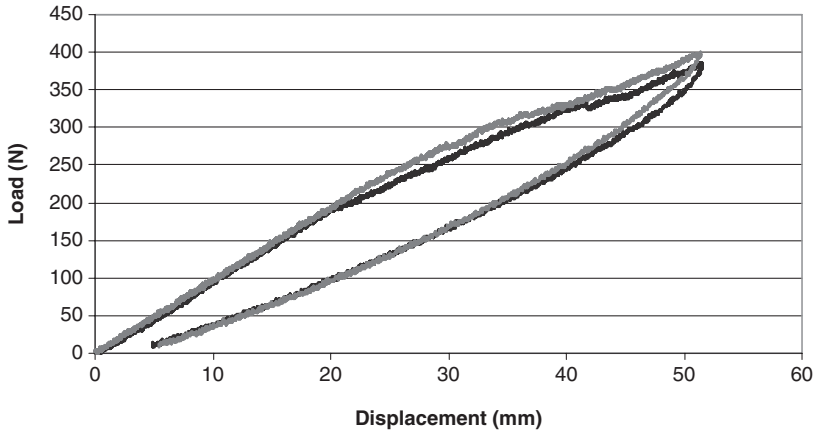

Figure 5. *Load vs displacement diagram for the Mode II test.*

FINITE ELEMENT ANALYSIS FOR MODE I

The purpose of performing the finite element analysis was to identify the correct physical models that represent the stitch interactions with the parent laminate and stitch failure mechanisms. The observations from the experiments and the test data were used in generating the models. Specifically, one is interested in strain energy release rate around the crack tip and stresses in the stitches in the bridging zone. The J-integral was used to calculate $G_{\text{c-par}}$ (parent G or strain energy release rate at the crack tip) by using a contour that does not include the stitches in the bridging zone. $G_{\text{c-eff}}$ (effective energy release rate) was also calculated by the J-integral contour, which included the stitches in the bridging zone. The comparison of $G_{\text{c-par}}$ and $G_{\text{c-eff}}$ will give us the effectiveness of stitching in laminated composites. The FEA modeling was performed at two levels, two-dimensional (2D) models and full three-dimensional (3D) simulation. The 2D solid model, which uses less computer resources, provides a fairly accurate displacement field. However, it cannot be used to accurately determine the stress field and the value of J-integral. We used the 3D shell elements to determine the stress field in each ply and the 3D solid element to calculate the J-integral. It should be pointed out that the midplanes of the 3D shell elements are different from ones used in regular laminated composites and the J-integral cannot be obtained using this model. J-integral obtained from the 3D solid model matches the experimental results well.

Specimen Description and Properties

The specimen was made up of 4 stacks. Each stack consisted of 7 plies, which were oriented at [45/−45/0/90/−45/45°]. The materials used in each stack have slightly different properties as shown in Tables 1 and 2.

The specimens were 178 mm long and 18.0 mm wide with 1600 denier Kevlar® stitches. Each stitch consists of two of the Kevlar yarns. The stitch density was $8 \times 1/5''$ which corresponded to 6.2 stitches/cm^2 (40 stitches/in.^{2}). The pitch or the distance between two

Table 1. Thickness, material, and ply orientation for each material stack.

Ply number	Thickness (mm)	Orientation (°)	Material system
1	0.161	45	AS4-3501-45
2	0.161	−45	AS4-3501-45
3	0.326	0	AS4-3501-00
4	0.178	90	AS4-3501-90
5	0.326	0	AS4-3501-00
6	0.161	−45	AS4-3501-45
7	0.161	45	AS4-3501-45

Table 2. Elastic constants for different stacks.

Material system	E_1 (GPa)	E_2 (GPa)	ν_{12}	G_{12} (GPa)	G_{13} (GPa)	G_{23} (GPa)
AS4-3501-45	103.7	11.03	0.34	5.52	5.52	3.58
AS4-3501-00	105.5	11.03	0.34	5.52	5.52	3.58
AS4-3501-90	102.6	11.03	0.34	5.52	5.52	3.58

adjacent stitches in the same row was 3.2 mm (1/8 in.), and the spacing between two adjacent stitch rows was 5.1 mm (1/5 in.).

J-integral, Parent G_c, and Effective G_c

J integral is defined as follows:

$$J = \int_{\Gamma} \left(U_0 n_1 - T_i \frac{\partial u_i}{\partial x_1} \right) ds \tag{1}$$

Here, U_0 is the strain energy density, n_1 is the x-component of the outer normal vector along the path shown in Figure 6 assuming crack propagation along the x-direction, u_i is the displacement along the i-direction and T_i is the component of the surface force along the i-direction.

In order to thoroughly understand the effect of the stitches, one should carefully examine the bridging zone, where the stitches partially connect the two ligaments of the laminate and prevent crack propagation. Three parameters, $G_{\text{c-eff}}$, $G_{\text{c-par}}$, and crack opening displacement (COD), can be used to characterize the stitch's effect on the bridging zone. The experimental methods of measuring the fracture toughness, e.g., DCB, ENF specimens, are useful, but the measured effective fracture toughness values are specific to the particular specimen configuration as the effective fracture toughness depends on the specimen thickness, laminate orientation, and stitch properties. The FE model, however, provides flexibility. In addition to $G_{\text{c-eff}}$, one can obtain $G_{\text{c-par}}$ and COD from the FE model. One can also easily change the model and adjust the parameters (such as the density of stitching and diameter of the stitches) to predict the effective fracture toughness without making new specimens. The J-integral is path independent when the crack

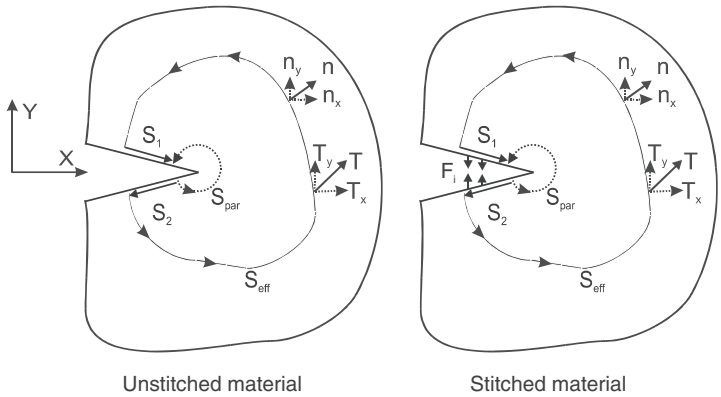

Figure 6. *Contours of J-integral including and excluding the stitches.*

surfaces are free of traction. However, due to the presence of stitches in the bridging zone, the two crack surfaces are not truly separated since they are still partially connected by the unbroken stitches. Hence, for stitched laminates, J-integral is path dependent when the bridging zone exists. If the path of the contour (S_{par}) is chosen to be very close to the crack tip and the load applied corresponds to crack propagation, J-integral should be equal to $G_{\text{c-par}}$, which is a parent material property regardless of whether the specimen is stitched or not. On the other hand, if the path of contour (S_{eff}) includes unbroken stitches in the bridging zone, the J-integral should be equal to $G_{\text{c-eff}}$, which should be larger than $G_{\text{c-par}}$ and will reach a constant value when the bridging zone is fully developed and the contour incorporates all the unbroken stitches in the bridging zone. Subsequently, as the crack continues to propagate, the bridging zone will eventually reach a constant length and move with the crack tip (steady state conditions). The dashed line of the contour in Figure 6 was used to calculate $G_{\text{c-par}}$ and the solid line of the path that includes all unbroken stitches in the bridging zone was used for calculating $G_{\text{c-eff}}$. For any closed curve (Figure 6), J-integral should be zero no matter whether the material is stitched or not, and it can be expressed as:

$$G_{S\text{-eff}} + G_{S1} - G_{S\text{-par}} + G_{S2} = 0 \tag{2}$$

Here S_{eff} is a contour which includes all stitches in the bridging zone, S_{par} does not include any stitches and is very close to the crack tip, S_1 is along the top crack surface and S_2 is along the bottom crack surface. For an unstitched material, there are no traction vectors (surface forces) on the two crack surfaces, and hence both G_{S1} and G_{S2} should be zero. Then from Equation (2), $G_{S\text{-eff}} = G_{S\text{-par}}$.

However, for a stitched material, there are some unbroken stitches in the bridging zone, which still connect the two crack surfaces together. The traction vectors are not zeros anymore and are applied by the unbroken stitches in the bridging zone.

The relationship between G_{par} and G_{eff} for Mode I can be expressed as:

$$G_{S1} + G_{S2} = \oint_{S1+S2} -T_i \frac{\partial u_i}{\partial x_1} ds = -2 \sum \left| \frac{\partial v}{\partial x} \right|_i \cdot F_i \tag{3}$$

Here v_i is the vertical displacement at the position of the stitch i and F_i is the force in the stitch i. Due to symmetry, the upper and lower integrals will be equal, and hence the factor 2 is applied in the above equation. Then we obtain

$$G_{I\text{-eff}} = G_{I\text{-par}} + 2\sum \left|\frac{\partial v}{\partial x}\right|_i \cdot F_i \tag{4}$$

Similarly for Mode II,

$$G_{I\text{-eff}} = G_{I\text{-par}} + 2\sum \left|\frac{\partial u}{\partial x}\right|_i \cdot F_i \tag{5}$$

Here u_i is the horizontal displacement at the position of the stitch i, and F_i is the axial force in the stitch i.

The interpretation of Equations (4) and (5) for discrete reinforcements will be the subject of a forthcoming paper. At present, we will use a simpler method in which the stitches are smeared over the bridging zone and the stitch forces are replaced by continuous traction. Then the summation in Equation (4) can be written as:

$$G_{I\text{-eff}} = G_{I\text{-par}} + \int_0^c p\frac{\partial v}{\partial x}dx \tag{6}$$

where c is the bridging length and the distributed forces $p(x)$ due to the stitches can be expressed in terms of the smeared stitch stiffness k as:

$$p(x) = 2kv(x) \tag{7}$$

In Equation (7), $2v$ represents the crack opening at a given distance x in the symmetric Mode I case. The foundation spring constant k can be related to the axial stiffness k_s of a single stitch as:

$$k = Nk_s = \frac{k_s}{bd} \tag{8}$$

where N is the number of stitches per unit area, and b and d are, respectively, the stitch row spacing and the number of stitches per unit length in a given row. Note that the dimension of k_s is force/length and that of k is force/length^3. Substituting (7) into (6) and performing the integration we obtain:

$$G_{I\text{-eff}} = G_{I\text{-par}} + \frac{1}{2}Nk_s(2v_c)^2 \tag{9}$$

where $2v_c$ is the crack opening displacement at the end of the bridging zone. Thus the difference between $G_{I\text{-eff}}$ and $G_{I\text{-par}}$ is actually the strain energy density (strain energy per unit area) of the stitches at the tip of the bridging zone. Similar results were obtained using analytical methods by Sankar and Dharmapuri [10].

2D Solid Modeling

MODELING PROCEDURE

After carefully observing Mode I specimens, we found that all stitches were broken without being pulled out. Test results also show that there was no ploughing action for Mode I and the average breaking strength for 1600 denier Kevlar was around 347 N with a failure strain of ≈5%. There were two yarns in one stitch; therefore, the average failure strength of each stitch was about 694 N. The same ultimate strength and strain can be used for all stitches and the stitch can be simply modeled as an elastic spring.

The parent laminates comprised 3D orthotropic materials, where material properties were strongly dependent on the fiber orientation with shear coupling in the laminates. In the 2D model, instead of specifying the detailed behavior of each individual layer, 'effective E_f' is used to represent the flexure modulus of the structure. The model was used to calculate the displacement of the laminates; and the strain and stress in the stitches. However, it cannot be used to obtain the stress distribution in each ply. One should be cautious when attempting to use this model to calculate the J-integral since it is directly related to the strain energy density and the gradient of the displacement. Later, the J-integral acquired from this 2D solid model will be verified using a full 3D simulation.

The specimen was assumed to have both geometric and material property symmetry about the middle surface and each ply was assumed linearly elastic with no shear coupling. In reality, there were +45 and −45° plies in laminates and shear coupling should exist.

The effective modulus can be easily calculated using the laminate theory as:

$$E_f = \frac{8}{h^3}\sum_{j=1}^{N/2}(E_x)_j(z_j^3 - z_{j-1}^3) \tag{10}$$

Here, N is the total number of plies and z_j is the distance from the neutral surface to the outside of the jth ply. E_x is the modulus along the x-direction and can be expressed as:

$$E_x = \frac{1}{(1/E_1)\sin^4\alpha + [-(2\nu_{12}/E_1) + (1/G_{12})]\sin^2\alpha\cdot\cos^2\alpha + (1/E_2)\sin^2\alpha} \tag{11}$$

$$\alpha = 45^\circ \rightarrow E_x = 14.54 \text{ (GPa)}$$
$$\alpha = 0^\circ \rightarrow E_x = 105.5 \text{ (GPa)}$$
$$\alpha = 90^\circ \rightarrow E_x = 11.03 \text{ (GPa)}$$

where, E_1, E_2, and G_{12} are the major modulus, minor modulus, and the shear modulus of each ply, respectively, and α is the angle between the major material axis and global x-axis. The effective modulus (E_f) of this specimen was equal to 47.78 GPa and was used in our 2D solid model.

Figure 2 shows the loading condition of the Mode I specimen, where all forces transferred from the loading fixture are moved to cross section A. As the crack propagates, the crack length L, measured to the crack tip at B, increases accordingly. Due to stable crack propagation, the total number of peak loads in the experiments matches the total number of broken rows of stitches (Figure 3). In this model, we used the critical loads as well as the corresponding crack length from experiment as input data to the FE model.

Table 3 lists the 10 peak loads and the corresponding 10 crack lengths from one of the Mode I tests.

It should be mentioned that the peak loads (P_1–P_{20}) and the crack lengths are obtained directly from the test data. The loads (F_x, F_y, M_z) at the cross section A are calculated by an iterative method based on the geometry of the loading fixture and the dimensions of the specimen.

Figure 7 shows the schematic drawing of the 2D solid model for the new Mode I test. The mesh around the crack tip is much denser than that of other areas and in this case, more accurate COD can be obtained around the crack tip. The stitches are connected on the top and bottom surfaces of the specimen. The position of the first row of stitches can be determined by trial and error until its strain reaches the failure strain under the critical load. The bending moment is applied through the equivalent couple $F_M(M_Z = F_M \cdot d)$. The corresponding location of each peak load was obtained directly from the test data.

Table 3. Input data for peak loads and corresponding crack lengths from one of the Mode I tests.

	P_1	P_3	P_5	P_8	P_{10}	P_{12}	P_{14}	P_{16}	P_{18}	P_{20}
Loads (N)	3176	3714	4523	5057	5417	4248	4688	5071	4786	5071
F_x (N)	806	918	1087	1184	1244	967	1046	1118	1034	1081
F_y (N)	1588	1857	2262	2528	2710	2124	2344	2536	2392	2536
M_z (N m)	13.37	9.39	5.18	0.69	−2.45	−2.47	−5.59	−7.83	−8.66	−10.07
Crack length h_5 (mm)	15.5	21.8	28.2	36.8	44.2	50.5	56.9	63.2	69.6	75.9

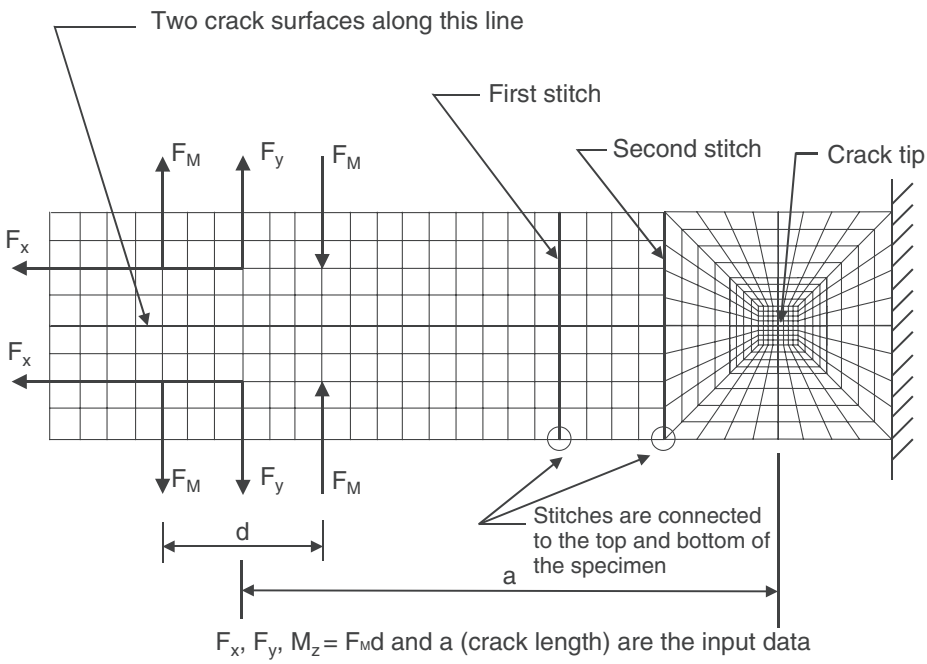

Figure 7. *Schematic of 2D solid model of stitched composites under Mode I.*

In the model, there was a total of 20 peak loads, which correspond to 20 locations of the broken rows of the stitches.

RESULTS FROM THE 2D SOLID MODEL

Figure 8 shows the principal strain distribution under the peak load P_1 (3176 N) and the crack length h_5 (15.5 mm). Although these strains are of no significance in fiber composites, the purpose of the figure is more to depict the FE model. There are two rows of stitches in the bridging zone. The maximum strain of the stitches in the bridging zone was 5.34%, which is approximately equal to the failure strain of a stitch.

The crack surface opening displacement (COD) versus distance behind the crack tip is shown in Figure 9. From a more detailed view in the vicinity of the crack tip, one can see

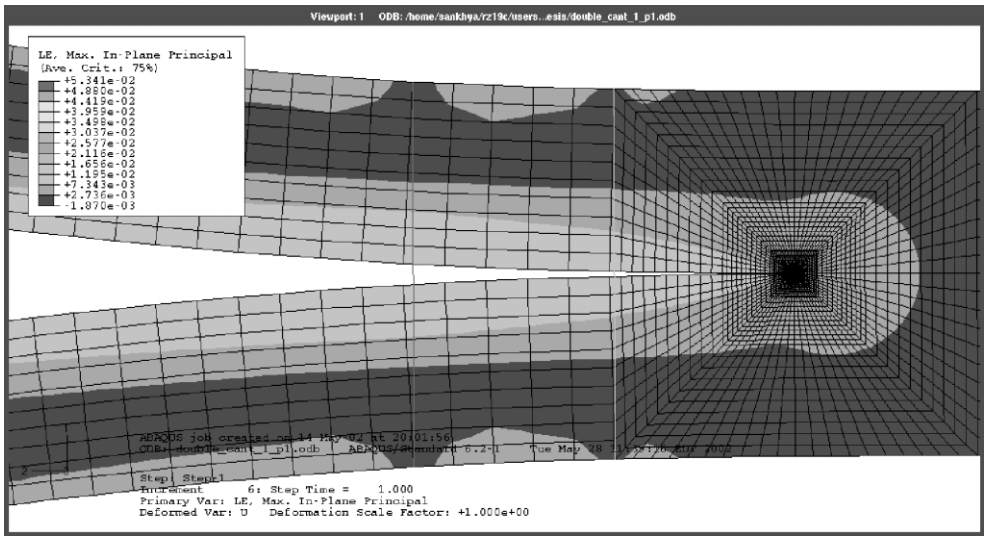

Figure 8. *Principal strain distribution in the 2D Model in Mode I analysis.*

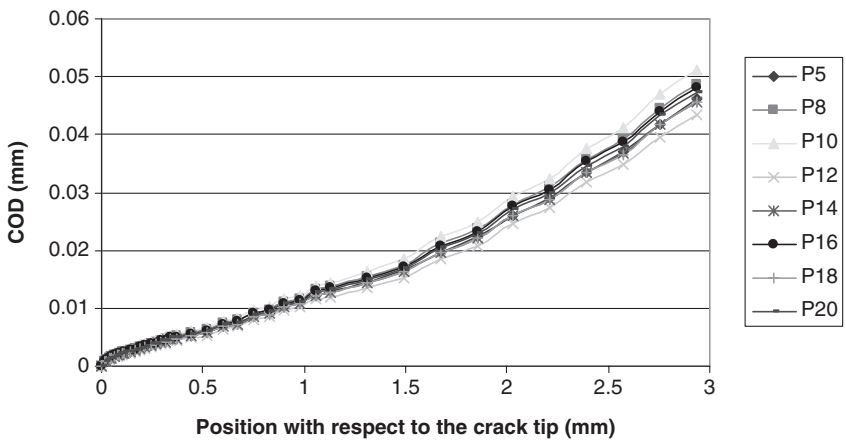

Figure 9. *Crack opening displacement (COD) vs distance from the crack tip for Mode I.*

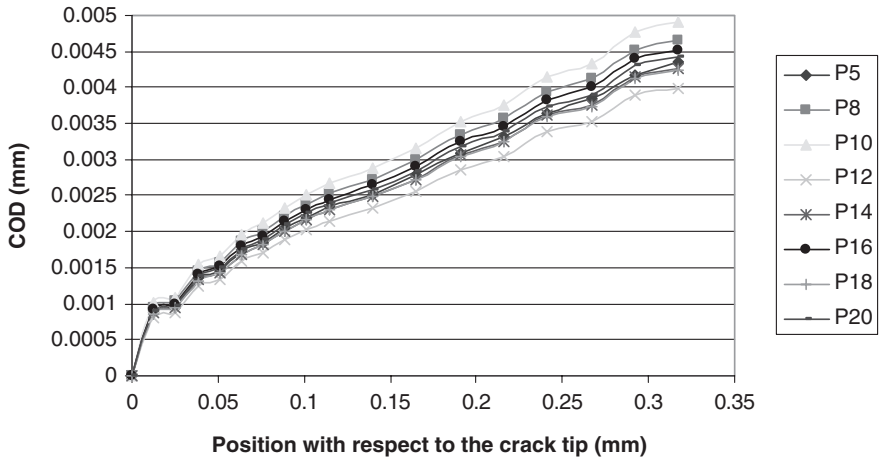

Figure 10. *COD vs distance close to the crack tip.*

Table 4. Values of $G_{IC\text{-}par}$ and $G_{IC\text{-}eff}$ under various loads.

	P_1	P_3	P_5	P_8	P_{10}	P_{12}	P_{14}	P_{16}	P_{18}	P_{20}
Loads (N)	3176	3714	4523	5057	5057	4248	4688	5071	4786	5071
$G_{c\text{-par}}$ (N/m)	473	560	735	875	980	630	735	823	578	630
$G_{c\text{-eff}}$ (N/m)	16,293	17,675	21,035	23,275	25,393	19,443	21,193	23,170	21,438	22,750

that CODs are almost the same (Figure 10) under various loading conditions. The stress intensity factor is directly related to COD which indicates that $G_{\text{Ic-par}}$ is approximately constant under various peak loads. $G_{\text{Ic-par}}$ is an intrinsic property of the parent material and this model verifies our assumption. When the location is close to the crack tip, COD versus location can be roughly expressed as $\delta_{\text{close}} = C_1\sqrt{x}$ (Figure 10) while moving away from the crack tip, the relationship between COD and the position is approximated as $\delta_{\text{away}} = C_2x^2$ (Figure 9). Table 4 gives the $G_{\text{Ic-par}}$ and $G_{\text{Ic-eff}}$ by using J-integral under various loading conditions. One can see that the values of $G_{\text{Ic-par}}$ are approximately constant, however $G_{\text{Ic-eff}}$ varies considerably.

Three-Dimensional Shell Element Modeling

MODELING PROCEDURE

The model described in section on ''2D Solid Modeling'' uses the effective E_f to represent the global flexural modulus of the structure, which provides realistic displacement values. However, the model cannot be used to obtain the stress field of each layer. Due to the symmetric geometry of the specimen and small shear coupling effect, 3D shell elements are an efficient choice. The 3D shell model used here is not like the traditional plate model. From Figure 11, one can see that instead of using the x–z plane, one uses the x–y plane as the midplane for 3D shell elements. Hence, there are a total of 28 midplanes for the 28 plies in this specimen and the 'thickness of the shell

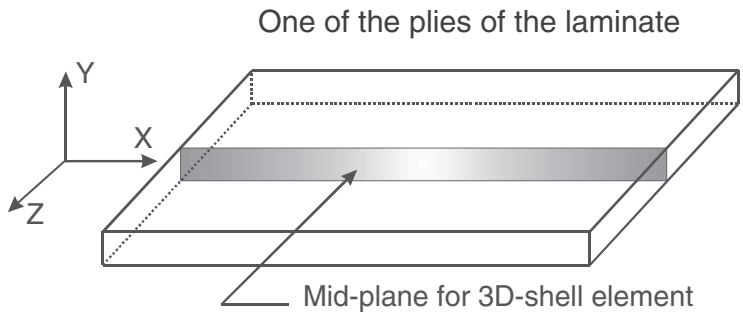

Figure 11. *Schematic drawing of the midplane for 3D-shell elements.*

Table 5. Material properties for the shell elements.

Material	E_x (GPa)	E_y (GPa)	ν_{12}	G_{xy} (GPa)	G_{xz} (GPa)	G_{yz} (GPa)
AS4-3501-00	103.7	11.03	0.34	5.52	5.52	3.58
AS4-3501-45	14.55	11.03	0.34	5.52	5.52	5.52
AS4-3501-90	11.03	11.03	0.34	5.52	5.52	5.52

element' is equal to the 'width of the specimen' (along the z-direction). Since each ply is oriented in the x–z plane, one must calculate E_x and E_y for each layer as the input properties for the 3D shell elements. Table 5 gives the material properties for 0, 45, and 90° layers. Unlike the 3D solid model, rotational degrees of freedom of the 3D shell model are active and the bending moment can be directly applied to the nodes. This is not an exact model for this structure but yields useful information about the stress field in each ply.

RESULTS AND DISCUSSION

The shell model is depicted in Figure 12. The peak load and corresponding crack length are 3185 N and 15.5 mm, respectively. By comparing to Figure 8 of the 2D solid model under the same loading conditions, one can note that the strain field is similar in both cases. The maximum stitch strains in the 2D solid model and the 3D shell model are 5.18% and 5.34%, respectively. The relative difference of these two maximum strains is about 3%. If one only needs to obtain strain and displacement fields, the 2D solid model is an efficient choice. Figure 13 gives the Mises stress distribution in the 3D shell model. Under this loading condition, the force of the first stitch in the bridging zone is 730 N and this stitch is about to break or has already broken. The maximum stress on the parent laminate is located in the zero degree layers with a value 1137 MPa and is less than the ultimate strength (1448 MPa) of the AS4-3501 material. As the stress in the stitch reaches the failure stress under this peak load, the maximum stress of the parent laminate is still well below the failure stress.

This model indicates that our new fixture can effectively break stitches and maintain the parent laminate intact. However, this 3D shell model cannot provide accurate J-integral around the crack tip. In order to obtain $G_{\text{Ic-par}}$ and $G_{\text{Ic-eff}}$, a full 3D model is needed to simulate the Mode I test.

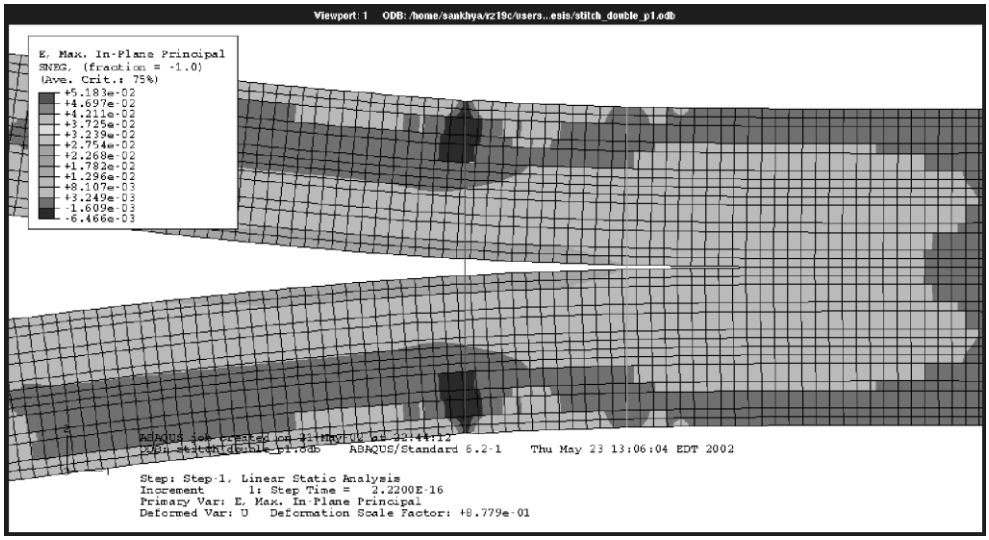

Figure 12. *Principal strain distribution in the 3D-shell model for Mode I.*

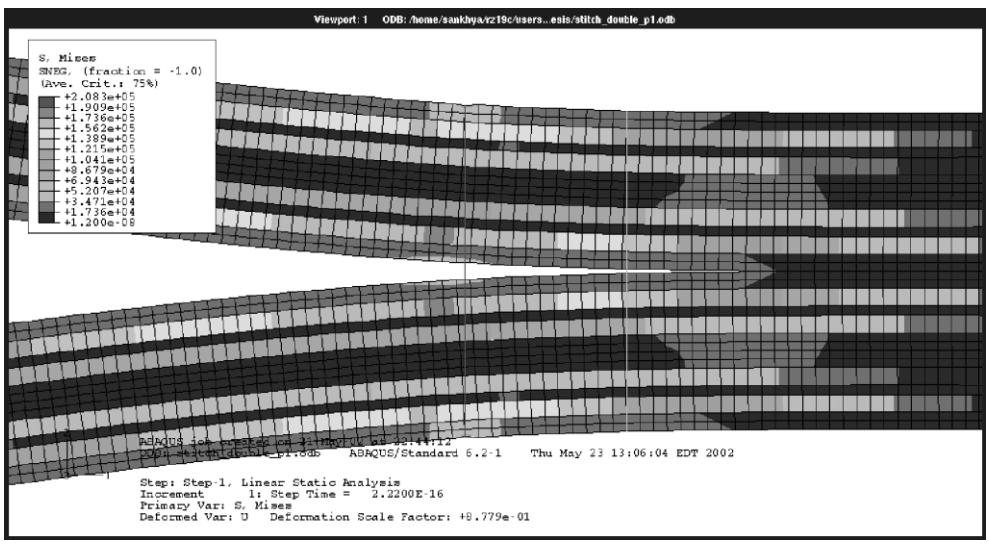

Figure 13. *Mises stress distribution in the 3D-shell model for Mode I.*

Three-dimensional Solid Model

In this model, the parent laminate was modeled using 3D orthotropic materials and stitches are modeled as bar elements. The material properties and orientation of the plies are shown in Tables 1 and 2. A total of 16,004 elements were used in this 3D model. Because the specimen undergoes large deformation, geometrically nonlinear analysis is used. Figure 14 shows the schematic drawing of the full 3D solid model of the new Mode I test.

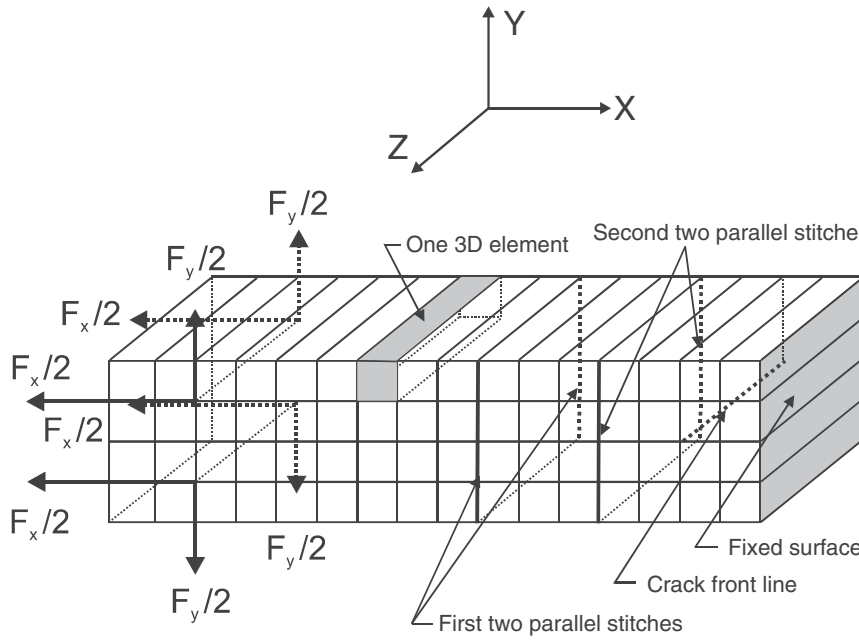

Figure 14. *Schematic drawing of the 3D solid model of the Mode I specimen.*

The positions of the stitches in the bridging zone are determined by the method used in the 2D solid model. Because the crack front is along a line, the J-integral is calculated through the two lines of the nodes – one represents the nodes on the 'front surface' (the nodes in front of the crack tip on the front surface) and the other as the nodes on the 'back surface' (the nodes in front of the crack tip on the back surface). In 3D solids, J-integral is not strictly path independent and the contour has to be shrunk to a point at the crack tip to obtain the G-value. However, since there are no significant gradients in the thickness direction in the present case, and hence the G can be obtained using an arbitrary contour as in-plane problems [25].

The 3D model can be used to verify the 2D model discussed in the previous section. Figure 15 gives the comparison of COD in both models under the same peak load P_{12}. When the position is very close to the crack tip, CODs from both models are almost identical. Moving away from the crack tip, the difference increases slightly and the maximum error is still $<8\%$. COD distributions under various peak loads are shown in Figure 16 and CODs are almost the same for different peak loads when the position is close to the crack tip. The stress intensity factor is directly related to COD and this model shows that the stress intensity factors ($K_{\text{Ic-par}}$) are approximately the same for various crack lengths.

From Table 6, one can note that the 2D and 3D model results do not agree well for G. The relative errors for $G_{\text{Ic-par}}$ and $G_{\text{Ic-eff}}$ can be as high as 88% and 50%, respectively. It should be mentioned that E_x is only 14.54 GPa for the 45° layers in the 3D model, while E_f (effective modulus) is 42.13 GPa in the 2D solid model. Thus approximating the laminate as a homogeneous continuum could have contributed to the errors in the J-integral.

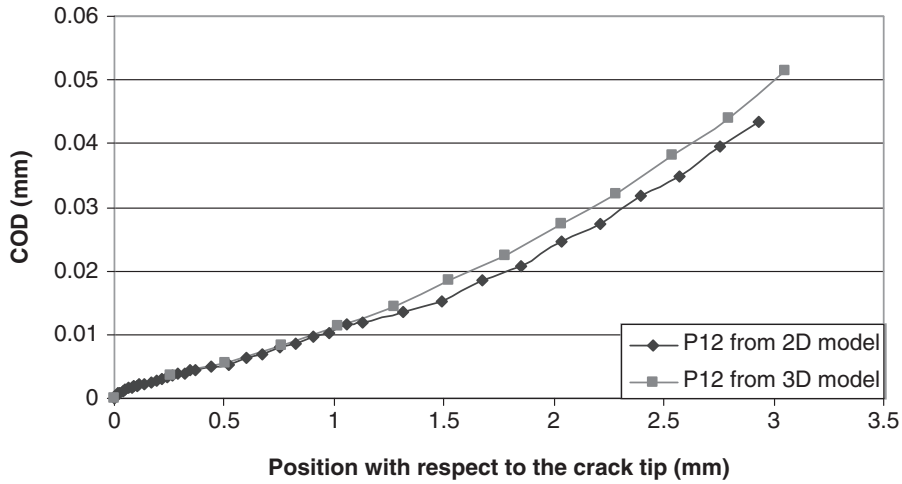

Figure 15. *Comparison of COD between 2D and 3D models.*

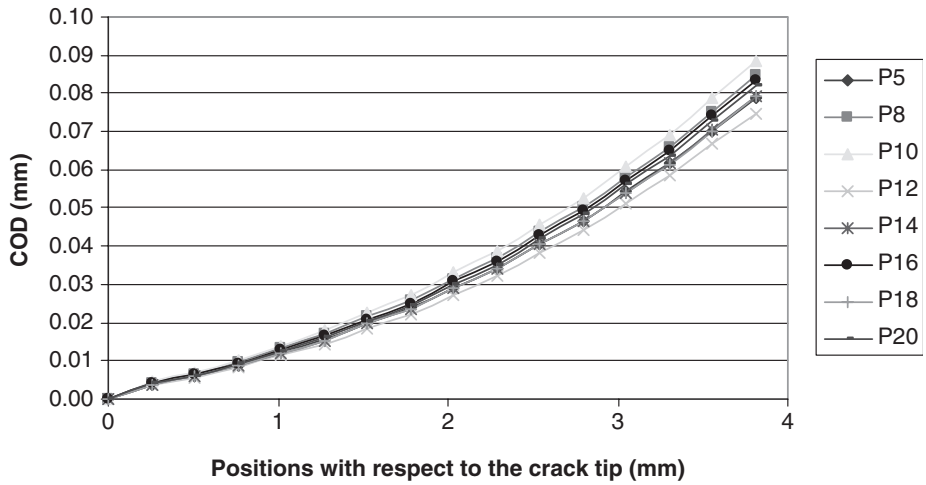

Figure 16. *Crack opening displacement vs position in the 3D model.*

Table 6. Comparison of $G_{Ic\text{-}par}$ and $G_{Ic\text{-}eff}$ between the 2D and 3D solid models.

	Load	P_1	P_3	P_5	P_8	P_{10}	P_{12}	P_{14}	P_{16}	P_{18}	P_{20}
3D Model	$G_{Ic\text{-}par}$ (N/m)	263	315	420	490	560	368	420	473	406	438
2D Solid	$G_{Ic\text{-}par}$ (N/m)	473	560	735	875	980	630	735	823	578	630
model	Relative error %	80.0	77.8	75.0	78.6	75.0	71.4	75.0	74.1	43.5	44.0
3D Model	$G_{Ic\text{-}eff}$ (N/m)	11,848	12,530	14,193	15,715	16,853	13,668	14,613	15,768	14,718	15,505
2D Solid	$G_{Ic\text{-}eff}$ (N/m)	16,293	17,675	21,035	23,275	25,393	19,443	21,193	23,170	21,438	22,750
model	Relative error %	37.9	41.1	48.2	48.1	50.7	42.3	45.0	46.9	43.9	45.6

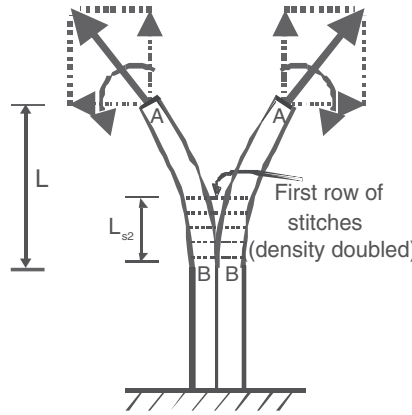

Figure 17. *Simulation of the specimen with the twice stitch density.*

Table 7. Effects of varying the stitch yarn cross section and the stitching density on $G_{Ic\text{-}eff}$.

Stitch parameters	$G_{Ic\text{-}eff}$ (N/m)	Increase in $G_{Ic\text{-}eff}$
1600 denier Kevlar yarn with a stitching density of 40 stitches/in.^{2}	12,600	–
1600 denier Kevlar yarn with a stitching density of 80 stitches/in.^{2}	16,100	28%
3200 denier Kevlar yarn and a stitching density of 40 stitches/in.^{2}	19,425	54%

Effect of Stitch Area of Cross Section and Stitch Density

The stitch cross-sectional area and the stitch density are the two most important factors that affect the effective fracture toughness in stitched laminates. The 3D model can be used to understand the effects of varying the stitch diameter and density on the effective fracture toughness.

First, the density of stitching is doubled and the stitch diameter is kept constant. In order to obtain the effective energy release rate $G_{\text{Ic-eff}}$, the intrinsic fracture toughness $G_{\text{Ic-par}}$ should be fixed. Loading conditions and the distance between the first stitch and the crack tip shown in Figure 17 were adjusted until the stress of the first stitch in the bridging zone reaches its ultimate strength and $G_{\text{Ic-par}}$ is equal to the value obtained from the original specimen. After the new bridging length (L_{s2} in Figure 17) and the new critical loading condition were determined, $G_{\text{Ic-eff}}$ was calculated.

Next, the cross-sectional area of the stitch yarn was doubled and the density of stitching was kept constant. Following the same procedures, the new L_{s2} and the new critical load were determined and $G_{\text{Ic-eff}}$ was calculated accordingly.

Table 7 provides results for these two simulations and it is apparent that increasing the cross-sectional area of the stitch has profound influence on $G_{\text{Ic-eff}}$. The effective fracture toughness $G_{\text{Ic-eff}}$ increases by 54% as the cross section is doubled, while it increases by 28% with doubling of the stitch density.

FINITE ELEMENT MODEL FOR MODE II

Modeling Procedure

Experiments reveal that for Mode II tests, there is a ploughing action between the stitches and the matrix [6]. Additionally, the stitches seem to undergo elastic-perfect plastic behavior before breaking. These observations were made during shear tests depicted in Figure 18.

In order to investigate the contribution of an individual stitch, a novel shear loading fixture was developed as shown in Figure 18. In this specimen, a Teflon film was placed in the entire interlaminar plane before curing. Thus, the shear load is transferred from one half of the specimen to the other half by the stitches. An extensometer was mounted to measure the relative displacement between the crack surfaces. When the relative displacement reached 0.08 mm, the load on a stitch reached the maximum value 299 N. The failure displacement was about 0.2 mm.

From the load–deflection diagram (Figure 19), one can note that the behavior of a stitch in Mode II loading is totally different from that in Mode I loading. In the Mode I test, there is no ploughing action between stitches and the parent laminate, however in Mode II, the stitches plough through the matrix which creates local damage in the parent laminate. Although the stitch itself does not undergo plastic deformation, the interaction of the stitch with the surrounding material can be represented by an elastic-plastic relation as shown in Figure 19. In order to represent this behavior, 'very short bar elements'

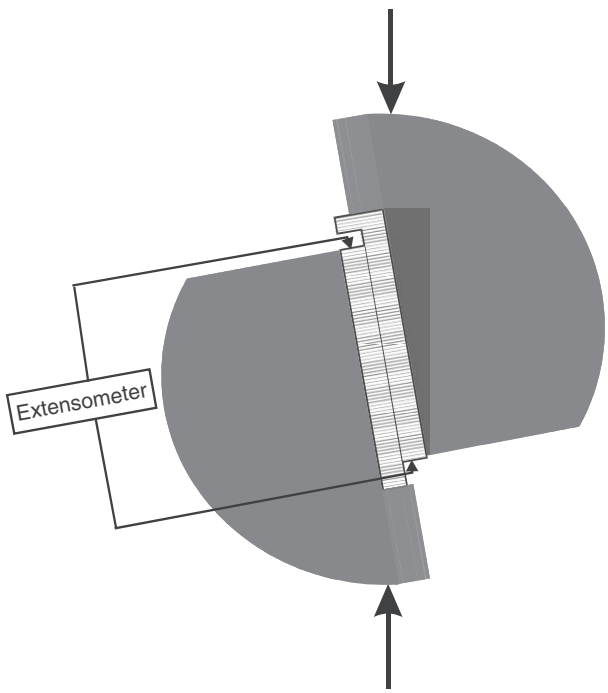

Figure 18. *Novel shear test to determine the behavior of stitches under shear loads.*

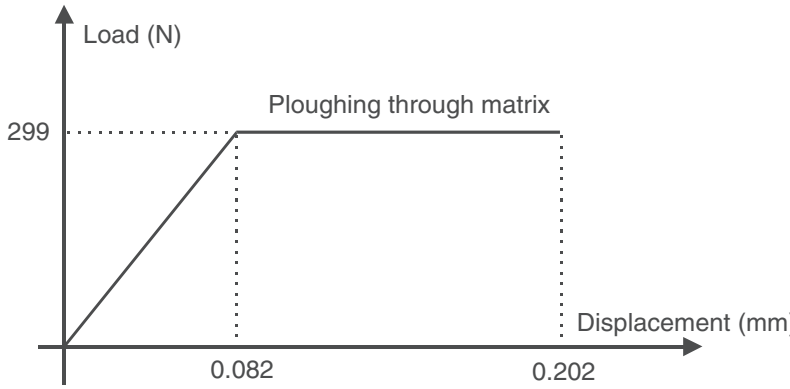

Figure 19. *Load–deflection relation for a stitch in Mode II specimens.*

Table 8. Loads and crack lengths for the Mode II test.

	P_1	P_2	P_3	P_4	P_5	P_6
Load (N)	140.6	176.6	207.7	233.1	218.4	279.3
Crack length (mm)	74.9	77.0	78.7	81.3	89.9	98.3

oriented along the crack surfaces are used to simulate the interaction between the stitches and the matrix. The length of the bar element was 0.125 mm and the stitch behavior can be idealized as an elastic-perfectly plastic material as shown in Figure 19.

The specimen used for the Mode II test was 165.1 mm long and 25.4 mm wide with an initial crack length of 74.9 mm. High-sensitivity Moiré interferometry was used to determine the crack lengths and the relative displacement between the two crack surfaces. Table 8 lists the six peak loads with respect to six different crack lengths. Similar to the case of Mode I, we can use the FE models to determine $G_{\mathrm{IIc\text{-}par}}$ and $G_{\mathrm{IIc\text{-}eff}}$.

Figure 20 shows the schematic drawing of the full 3D solid model of the Mode II test. It should be emphasized that the number of the stitches in the bridging zone depends on the crack length and the loading conditions. For instance, under the peak load P_5, there are 3 rows of the stitches in the bridging zone while under the peak load P_6, there are 4 rows of the stitches in the bridging zone.

Results and Discussion

Figure 21 shows CODs under three peak loads when the position is very close to the crack tip. They are almost the same. These results, again, verify our assumption – that $G_{\mathrm{IIc\text{-}par}}$ is a parent material property.

Table 9 presents the comparison of $G_{\mathrm{IIc\text{-}par}}$ and $G_{\mathrm{IIc\text{-}eff}}$ under different loading conditions. The effective Mode II fracture toughness is strongly dependent on the crack length and the number of stitches in the bridging zone. Usually, the more stitches that are involved in the bridging zone, the larger the $G_{\mathrm{IIc\text{-}eff}}$. We expect that as the crack continues to grow, the first row of stitches will finally break and at this moment, the bridging zone

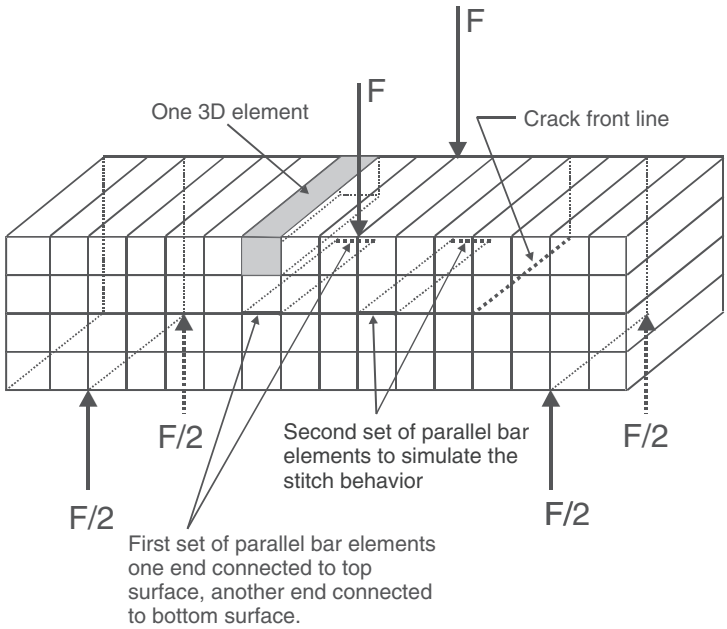

Figure 20. *Schematic drawing of 3D solid model for Mode II specimens.*

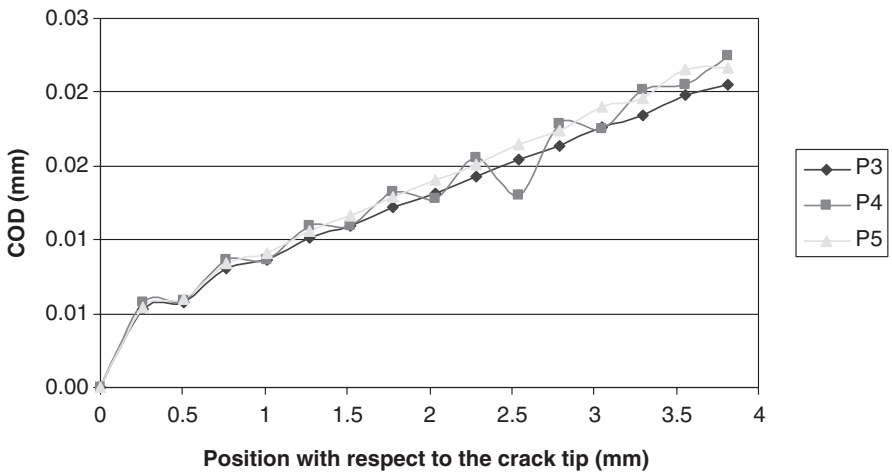

Figure 21. *Crack opening displacement in Mode II specimens at different loads.*

Table 9. Comparison of $G_{IIc\text{-}par}$ and $G_{IIc\text{-}eff}$ under different loading conditions.

Load	P_1	P_2	P_3	P_4	P_5	P_6
$G_{IIc\text{-}par}$ (N/m)	245	298	280	333	296	228
$G_{IIc\text{-}eff}$ (N/m)	298	543	718	1015	928	683

will reach its maximum length. After that, $G_{IIc\text{-}eff}$ will reach the maximum value and will remain approximately constant as the crack continues to propagate.

CONCLUSIONS

Two new test fixtures were developed to determine the effective Mode I and Mode II fracture toughness of stitched composites and the test data was used to obtain $G_{c\text{-}eff}$ by the conventional area method. Two parameters ($G_{c\text{-}par}$ and $G_{c\text{-}eff}$) were proposed to represent the fracture toughness of stitched composites. Several FE models were developed to characterize the behavior of stitched composites. Two-dimensional solid models yielded good displacement fields while 3D shell element provided the accurate stress fields in each ply. Computational requirements were low for both 2D solid model that uses homogenized material properties and 3D shell element. However, $G_{c\text{-}par}$ and $G_{c\text{-}eff}$ can be accurately determined only using a 3D solid model that model the individual layers. The J-integral around a contour that is very close to the crack tip yields the intrinsic fracture toughness of the composite material system. A contour that includes all the unbroken stitches yields the effective fracture toughness of the stitched laminate. From the 3D simulation, it has been found that increasing the cross-sectional area of the stitches is more effective in increasing the fracture toughness than increasing the density of stitching.

ACKNOWLEDGEMENTS

This research was supported by the NSF Grant CMS-9732887 to the University of Florida. The authors are thankful to Dr. D.R. Ambur and Mr. D.M. McGowan of NASA Langley Research Center for the stitched composite specimens, and for their support and encouragement.

REFERENCES

1. Mignery, L.A., Tan, T.M. and Sun, C.T. (1985). The Use of Stitching to Suppress Delamination in Laminated Composites, In: *ASTM STP 876*, pp. 371–385, American Society for Testing and Materials, Philadelphia.
2. Dexter, H.B. and Funk, J.G. (1986). Impact Resistance and Interlaminar Fracture Toughness of Through-the-thickness Reinforced Graphite/Epoxy, AIAA Paper 86-1020-CP, pp. 700–709.
3. Ogo, Y. (1987). The Effect of Stitching on In-plane and Interlaminar Properties of Carbon-epoxy Fabric Laminates, CCM Report Number 87-17, Center for Composite Materials, University of Delaware, Newark, May 1987, pp. 1–188.
4. Pelstring, R.M. and Madan, R.C. (1989). Stitching to Improve Damage Tolerance of Composites, In: *34th International SAMPE Symposium*, May 1989, pp. 1519–1528.
5. Dransfield, K.A., Jain, L.K. and Mai, Y.-W., (1998). On the Effects of Stitching in CFRPS–I. Mode I Delamination Toughness, *Composites Science and Technology*, **58**: 815–827.
6. Sharma, S.K. and Sankar, B.V. (1995). Effects of Through-the-thickness Stitching on Impact and Interlaminar Fracture Properties of Textile Graphite/Epoxy Laminates, NASA Contractor Report 195042, February, 1995.

7. Jain, L.K. and Mai, Y.-W. (1994). Mode I Delamination Toughness of Laminated Composites with Through-thickness Reinforcement, *Applied Composite Materials*, **1**(1): 1–17.
8. Jain, L.K. (1994). On the Effect of Stitching on Mode I Delamination Toughness of Laminated Composites, *Composites Science and Technology*, **51**: 331–345.
9. Jain, L.K., Dransfield, K.A. and Mai, Y.-W. (1998). Effect of Reinforcing Tabs on the Mode I Delamination Toughness of Stitched CFRPs, *Journal of Composite Materials*, **32**(22): 2016–2041.
10. Sankar, B.V. and Dharmapuri, S.M. (1998). Analysis of a Stitched Double Cantilever Beam, *Journal of Composite Materials*, **32**(24): 2203–2225.
11. Chen, L.-S., Ifju, P.G., Sankar, B.V. and Wallace, B. (1999). A Modified DCB Test for Composite Laminates with High-density Stitches, In: *Proceedings of the American Society for Composites, Fourteenth Technical Conference*, Bethel, CT, Sept. 27–29, 1999, pp. 214–217.
12. Chen, L.-S., Sankar, B.V., and Ifju, P.G. (2001). A Novel Double Cantilever Beam Test for Stitched Composite Laminates, *Journal of Composite Materials*, **35**(13): 1137–1149.
13. Chen, L.-S., Sankar, B.V. and Ifju, P.G. (2002). A New Mode I Fracture Test for Composites with Translaminar Reinforcements, *Composites Science and Technology*, **62**: 1407–1414.
14. Jain, L.K. and Mai, Y.-W. (1995). Determination of Mode II Delamination Toughness of Stitched Laminated Composites, *Composites Science and Technology*, **55**(3): 241–253.
15. Massabo, R. and Cox, B.N. (1999). Concepts for Bridged Mode II Delamination Cracks, *Journal of the Mechanics and Physics of Solids*, **47**: 1265–1300.
16. Jain, L.K., Drandfield, K.A. and Mai, Y.-W. (June 1998). On the Effects of Stitching in CFRPs – II. Mode II Delamination Toughness, *Composites Science and Technology*, **58**(6): 829–837.
17. Clara, S. and Barry D.D. (2000). Evaluation of the Accuracy of the Four-point Bend End-notched Flexure Test for Mode II Delamination Toughness Determination, *Composites Science and Technology*, **60**: 2137–2146.
18. Sih, G.C. and Liebowitz, H. (1968). Mathematical Theories of Brittle Fracture, In: Liebowitz, H. (ed.), *Fracture and Advance Treatise*, Vol. II, Academic Press, New York and London.
19. Ding, W. and Kortschot, M.T. (Aug. 1999). Simplifed Beam Analysis of the End Notched Flexure Mode II Delamination Specimen, *Composite Structures*, **45**(4): 271–278.
20. Massabo, R., Mumm, D.R. and Cox, B.N. (1998). Characterizing Mode II Delamination Cracks in Stitched Composites, *International Journal of Fracture*, **92**: 1–38.
21. Sankar, B.V. and Sonik, V. (1995). Modeling End-notched Flexure Tests of Stitched Laminates, In: *Proceedings of the American Society for Composites – Tenth Technical Conference*, Technomic Publishing Co., Lancaster, Pennsylvania, pp. 172–181.
22. Sonik, V. and Sankar, B.V. (1996). Modeling the Effects of Translaminar Reinforcements on Mode II fracture Toughness, In: *Proceedings of the Aerospace Division*, AD-Vol. 52, pp. 61–69, American Society of Mechanical Engineers, New York.
23. Chen, L.-S., Sankar, B.V. and Ifju, P.G. (2001). Mode II Fracture Toughness of Stitched Composites, In: *AIAA Structures, Structural Dynamics & Materials Conference*, Seattle, Washington, April 2001, AIAA Paper 2001-1483.
24. Post, D., Han, B. and Ifju, P.G. (1994). High Sensitivity Moiré: Experimental Stress Analysis for Materials, In: *Mechanical Engineering Series*, Springer-Verlag, New York, NY.
25. Sankar, B.V. and Sonik, V. (1995). Pointwise Energy Release Rate in Delaminated Plates, *AIAA Journal*, **33**(7): 1312–1318.